JOURNAL OF SPACECRAFT AND ROCKETS
Vol. 32, No. 1, January–February 1995

Effects of g Jitter on Free-Surface Motion in a Cavity

Y. Kamotani,* L. Chao,† S. Ostrach,‡ and H. Zhang†
Case Western Reserve University, Cleveland, Ohio 44106

Lateral g-jitter effects on free-surface deformation are studied numerically in a zero-gravity environment for liquids in an open square container. In order to allow for different contact-line conditions, a hysteresis parameter is incorporated into the SOLA-SURF finite difference scheme. The resonant frequencies of the free-surface motion are computed under various conditions. The resonant frequency is largest when the contact line is fixed and decreases as it is allowed to move. The effect of viscosity reduces the resonant frequency or damps the resonance. The motion of the free surface and the amplitude of its deformation are investigated for two types of g jitter (sinusoidal and impulsive) that are typically encountered aboard a spacecraft. It is shown that relatively large deformation occurs if the frequency of the periodic g jitter is near the resonant frequency. The impulsive g jitter excites capillary waves with the resonant frequency, but they decay with time. Based on the computation and a scaling analysis, the amplitude of the free-surface deformation is expressed in useful dimensionless form for those two types of g jitter.

Nomenclature

A	= amplitude of container vibration, m
Bo	= Bond number
$c, \bar{c}$	= dimensionless constants
g	= acceleration level for impulsive g jitter, m/s^2
g_0	= gravitational acceleration on Earth, m/s^2
h	= dimensionless height function
h_0	= dimensionless static height function
ℓ	= dimensionless length scale for viscous stresses
L	= length scale (container size), m
Oh	= Ohnesorge number
p	= dimensionless pressure
t	= dimensionless time
t^*	= dimensional time, s
t_0	= dimensionless duration of impulsive g jitter
(u, v)	= dimensionless velocity components
(u^*, v^*)	= dimensional velocity components, m/s
(x, y)	= dimensionless coordinates defined in Fig. 1
x^*	= dimensional coordinate, m
w	= dimensional frequency, s^{-1}
U	= reference velocity, m/s
Γ	= dimensionless hysteresis parameter defined in Eqs. (8) and (9)
Δ	= dimensionless free-surface deformation for periodic g jitter
Δ_0	= dimensionless free-surface deformation for impulsive g jitter
Δ_0^*	= dimensional free-surface deformation for impulsive g jitter, m
μ	= fluid dynamic viscosity, Pa-s
ν	= fluid kinematic viscosity, m/s^2
ρ	= fluid density, kg/m^3
σ	= surface tension, N/m
τ	= dimensional time, s
τ_0	= dimensional duration of impulsive g jitter, s
ω	= dimensionless frequency
ω_n	= dimensionless resonant frequency

Received Nov. 10, 1993; revision received May 5, 1994; accepted for publication May 16, 1994.

*Professor, Department of Mechanical and Aerospace Engineering. Associate Fellow AIAA.

†Research Associate, Department of Mechanical and Aerospace Engineering.

‡Professor, Department of Mechanical and Aerospace Engineering. Fellow AIAA.

Introduction

IT is known that containerless materials being processed in a microgravity environment may be influenced by two effects, neither of which can be easily controlled.[1] The first effect is thermocapillary convection, and the second effect, which can be serious under some conditions, is the spacecraft vibration (g jitter) from a number of sources.[2] Both thermocapillary convection and g-jitter-generated flow are influenced by free-surface motion, and they can interact with each other. The susceptibility of crystal melts to g-jitter disturbances not only increases the displacement of the free surface, but also changes the steady heat transfer during the material processing to an irregular one, which may adversely influence the crystal quality. It is therefore important to study the free-surface motion induced by g jitter and the associated bulk fluid motion.

In the present investigation, unlike the extensive experimental and analytical studies of the dynamics of liquid fuel in fuel tanks of aircraft conducted during the 1960s,[3] the capillary force is not negligible, but a dominant force in a weak gravitational field. While there exist some classical linear and nonlinear inviscid studies of standing capillary waves in a finite-depth container,[4–6] those models are not adequate for the description of current systems with strong viscous and hysteresis effects. Several studies have dealt with g-jitter-induced convection in a completely enclosed container.[7–9] However, in microgravity containerless material processing, the dynamics of the free surface cannot be ignored. For a liquid in a container with a free surface, g jitter can cause surface disturbances and associated bulk fluid motion. A contact line is formed at the intersection of the free surface and the container wall, and its behavior significantly affects the dynamics of the free surface. In the linearized finite element study of surface waves by Curvelier,[10] while the dependence of resonant frequencies on viscous effects was shown, the contact angle was fixed at 90 deg and no other contact-line conditions or nonlinear effects were considered. In the maker-and-cell dimensional calculation of the axisymmetrical sloshing in a low-gravity condition by Veldman and Vogel,[11] the contact angle was fixed at 90 or 0 deg, and the dependence of resonant frequencies on the contact angle was shown. However, no variation of the dynamic contact angle was allowed during the sloshing in their calculations. More recently, numerical simulations were conducted to study the effects of g jitter and thermocapillary convection on float zones,[12] but free-surface deformation was not considered. Alexander and Zhang[13] analyzed numerically the convection in float zones with free-surface motion due to g jitter. The contact line was fixed in their analysis, and the free-surface shape was demonstrated to be sensitive to g jitter.

The present study is concerned with liquid free-surface motion in an open rectangular container subjected to g jitter in the direction

parallel to the free surface. The free surface is known to be most sensitive to g jitter in that direction.[14]

In the present problem, the contact-line conditions are represented by a hysteresis parameter that indicates the "hysteresis degree" of the contact line. In this representation, the contact line is allowed to move and the contact angle is allowed to change during the g-jitter disturbance. By using the modified SOLA-SURF code, full transient Navier-Stokes calculations are performed to obtain quantitative results and to identify many system characteristics. The present paper is based on Ref. 15.

Basic Equations and Boundary Conditions

Consider an open square container holding liquid that moves according to $A \sin wt$ in the x direction (see Fig. 1). The conservation equations are formulated in a noninertial reference frame attached to the container. Then the effect of the container motion appears as body-force terms, called g-jitter terms, in the equations of motion. Such periodic g gitter is caused aboard a spacecraft by various sources such as rotating equipment, structural oscillations of the spacecraft, and, in the case of manned spacecraft, astronauts' exercise on a bicycle or a treadmill. This type of g jitter is important in the present problem, since, as will be shown later, it can cause large free-surface deformation. Primitive variable forms of conservation equations are employed so that it is easier to implement the free-surface stress boundary conditions. Typically aboard a spacecraft the periodic g-jitter level is 100 to 1000 times larger than the steady g level; thus, relative to the free-surface deformation due to the periodic g jitter, the deformation before the start of the g jitter is very small. Therefore, the initial free-surface shape is determined by the static contact angle at the wall. In the present analysis the static contact angle is assumed to be 90 deg; as a result, the initial shape becomes flat. This assumption is made so that we can use rectangular coordinates, which greatly simplifies the present analysis. The flat shape can also be obtained by pinning the contact lines at the edges of the container and adjusting the fluid volume in the container, as was done in our past microgravity experiment on thermocapillary flow,[14] in conjunction with which the present work was conducted. The flow is assumed to be incompressible with constant physical properties. Since relatively small deformation is of interest in the present study, the fluid motion is assumed to be laminar and two-dimensional. The velocity scale U is chosen from the balance of the inertial force (which scales with $\rho U^2/L$) and the surface tension force (σ/L^2), since the dimensionless resonant frequencies ω_n are nearly fixed except for a small shift due to viscous effects. Therefore, the length, time, velocity, pressure, and frequency are nondimensionalized by L, $(\rho L^3/\sigma)^{\frac{1}{2}}$, $(\sigma/\rho L)^{\frac{1}{2}}$, σ/L, and $2\pi(\sigma/\rho/L^3)^{\frac{1}{2}}$, respectively. The dimensionless governing equations can then be written as

$$\frac{\partial u}{\partial x} + \frac{\partial v}{\partial y} = 0 \tag{1}$$

$$\frac{\partial u}{\partial t} + u\frac{\partial u}{\partial x} + v\frac{\partial u}{\partial y} = -\frac{\partial p}{\partial x} + Oh \cdot \left(\frac{\partial^2 u}{\partial x^2} + \frac{\partial^2 u}{\partial y^2}\right) + Bo \sin(2\pi\omega t) \tag{2}$$

$$\frac{\partial v}{\partial t} + u\frac{\partial v}{\partial x} + v\frac{\partial v}{\partial y} = -\frac{\partial p}{\partial y} + Oh \cdot \left(\frac{\partial^2 v}{\partial x^2} + \frac{\partial^2 v}{\partial y^2}\right) \tag{3}$$

The dimensionless parameters appearing in the above equations are defined as

$$\text{Ohnesorge number } Oh = \frac{\mu}{(\rho\sigma L)^{\frac{1}{2}}}$$

$$\text{Bond number } Bo = \frac{\rho L^2 A w^2}{\sigma}$$

Oh represents the ratio of the viscous (damping) force to the surface-tension (stabilizing) force, and Bo represents the ratio of the g-jitter force to the surface-tension force.

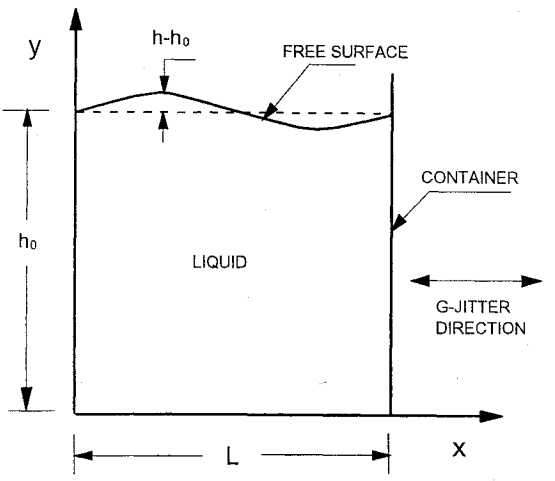

Fig. 1 Configuration and coordinate system.

At the rigid walls, we have the no-slip boundary condition

$$u = v = 0 \tag{4}$$

The no-slip condition does not apply to the contact line, which is allowed to move along the wall.

At the free surface, we have the kinematic boundary condition and the normal and tangential stress balance equations as follows:

$$\frac{\partial h}{\partial t} + u\frac{\partial h}{\partial x} = v \tag{5}$$

$$p = 2\,Oh \frac{1 + (\partial h/\partial x)^2}{1 - (\partial h/\partial x)^2} \cdot \frac{\partial v}{\partial y} - \frac{\partial^2 h/\partial x^2}{[1 + (\partial h/\partial x)^2]^{\frac{3}{2}}} \tag{6}$$

$$\frac{\partial u}{\partial y} = -\frac{\partial v}{\partial x} - \frac{4(\partial h/\partial x)(\partial v/\partial y)}{1 - (\partial h/\partial x)^2} \tag{7}$$

where h is the free-surface height function. Equation (6) is the normal stress balance equation, and Eq. (7) is the tangential balance equation.

The conditions at the contact lines are very complex. Although the static contact angle is assumed to be 90 deg in the present problem, it does not remain constant in general during the unsteady motions of the fluid and the contact lines. The contact-line behavior depends on various factors, such as the wetting conditions, the wall roughness, and the fluid motion. In the case where the dynamic free-surface location deviates only slightly from the static shape, Satterlee and Reynolds[16] introduced a hysteresis parameter to provide a macroscopic way to include those factors. As free-surface deformation is relatively small in the present analysis, we simplify the contact-line conditions by adopting the hysteresis parameter and impose the following conditions:

$$\frac{\partial h}{\partial x} = \Gamma \cdot (h - h_0) \tag{8}$$

$$\frac{\partial h}{\partial x} = -\Gamma \cdot (h - h_0) \tag{9}$$

Equation (8) is for the upper left corner, and Eq. (9) is for the upper right corner. The static height function h_0 is assumed to be constant (= 1) in this study. The hysteresis parameter Γ is a dimensionless parameter. When Γ is zero, the contact angle is fixed and the contact line is free to move, whereas when Γ is infinite, the contact line is fixed but the dynamic contact angle is allowed to vary. The free-surface shapes for various values of Γ are sketched in Fig. 2. The experimental data of Satterlee and Reynolds,[16] and Reynolds and Satterlee,[17] taken under various conditions and with various materials, fall between $\Gamma = 0$ and $\Gamma = \infty$.

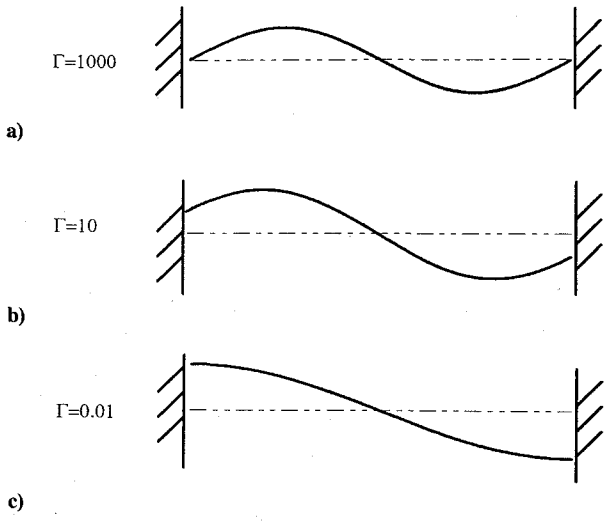

Fig. 2 Fundamental resonant modes for three values of Γ.

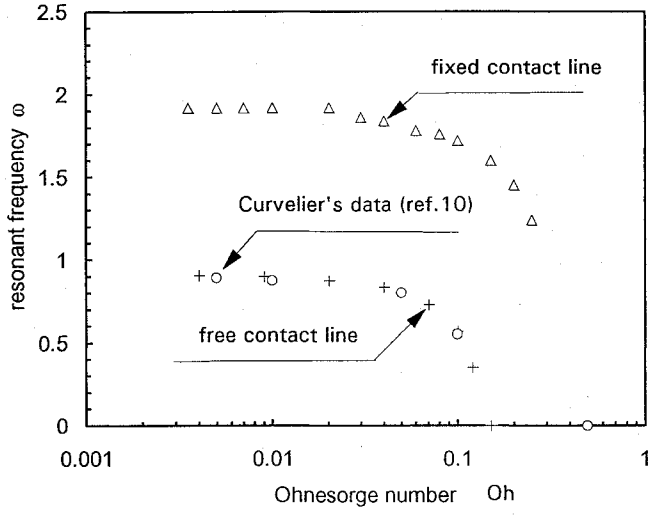

Fig. 3 Dependence of resonant frequency on Ohnesorge number.

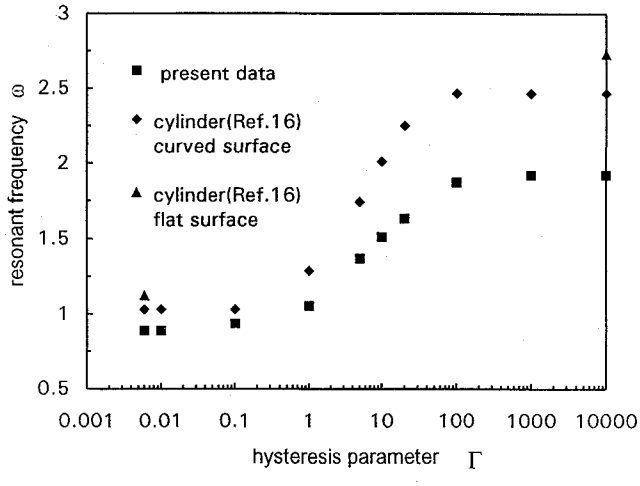

Fig. 4 Effect of contact-line hysteresis on resonant frequency.

Solution Procedure

The SOLA-SURF finite-difference solution algorithm is chosen to solve the present transient free-surface flow.[18,19] This scheme is an explicit one that uses a height function to describe the free-surface motion. Since we are concerned with the transient flow behavior and the amount of free-surface deformation is relatively small in the present study, this explicit scheme is appropriate. In each step, the pressure and velocities are iterated simultaneously, and the Dirichlet free-surface pressure boundary condition [Eq. (6)] is directly incorporated into the iteration procedure. Since Eq. (6) is satisfied only at the free surface, whose location does not necessarily coincide with the center of the surface cell where the pressure is defined, interpolation or extrapolation is made in the surface cell in order to insure that the capillary effect applies at the exact location. The interpolation or extrapolation in the surface cell is made with the aid of the height function, which is calculated from the last time step. After both new pressure and new velocities are known, the new height function is calculated by the Crank-Nicholson finite differencing of the kinematics [Eq. (5)], and hence the contact-line conditions (8) and (9) are the Robin (mixed) boundary conditions for Eq. (5). Finally, after the new height function is calculated, a cubic-spline-fitting method is used to determine the curvature in Eq. (6), which is needed at the next time step.

For oscillatory flow over a flat plate it is known[20] that the dimensionless boundary-layer thickness along the wall is about $9.0(\nu/\omega L^2)^{\frac{1}{2}}$, which can be expressed as $9.0(Oh/\omega)^{\frac{1}{2}}$. As the smallest boundary-layer thickness in the present study is about 0.2, a 20×20 uniform mesh is very adequate for the present analysis. A more detailed discussion of the grid-size effect is given in Ref. 15. Also in Ref. 15, the free surface motion due to periodic g jitter for a viscous-dominated case is analyzed theoretically, and the approximate analytical solution is shown to agree well with the present numerical result. In the present numerical scheme, the free-surface deformation must be within one numerical grid for stability, which limits the mesh size. With the uniform 20×20 mesh, the amount of surface deformation is limited to less than 5% of the container size.

Results and Discussion

Resonant Frequencies

Since it is important to know the resonant frequencies of the system before we discuss the effect of g jitter, they are computed under various conditions. As will be discussed later, simple sloshing motion of the fluid is of main interest in the present study; thus only the resonant frequencies for the mode (see Fig. 2) are presented herein. The value of each resonant frequency is determined by specifying an initial free-surface shape and observing the subsequent motion of the free surface without g jitter. With $Bo = 0$, Eqs. 1–9 show that the fluid motion depends on Oh and Γ.

In Fig. 3 the dependence of the resonant frequency ω_n on Oh is shown for the fixed-contact-line condition (Γ is set equal to 1000) and for the free-contact-line condition ($\Gamma = 0$). The resonant frequency for $\Gamma = 1000$ is about twice as large as that for $\Gamma = 0$ for a given Oh. When Oh becomes larger than about 0.15 for $\Gamma = 0$ and 0.3 for $\Gamma = 1000$, the viscous effect from the walls becomes dominant, so that the initial surface displacement decays monotonically, which is considered as zero frequency. On the other hand, when Oh is less than about 0.01, the wall effect becomes small and the resonant frequency becomes equal to that for inviscid flow ($Oh = 0$), although the fluid motion will decay slowly if Oh is not exactly zero. The results of analysis by Curvelier[10] for $\Gamma = 0$ are also shown in Fig. 3, and good agreement with the present results is shown.

The effect of Γ on the resonant frequency is shown in Fig. 4 for $Oh = 0.01$ (nearly inviscid case). The frequency up to about $\Gamma = 0.01$ is equal to that for the free contact line; the resonant frequency then increases with Γ up to about $\Gamma = 1000$, beyond which it is equal to that for the fixed-contact-line condition ($\Gamma = \infty$). Satterlee and Reynolds[16] computed the resonant frequencies for an open cylindrical container by the variational method. Their results for a concave free surface (static contact angle = 60 deg) and for a flat surface are shown in Fig. 4. The effect of Γ has the same trend as in the present cavity configuration, although the resonant frequency is generally higher in the cylindrical configuration. The ratio of the resonant frequency for $\Gamma = \infty$ to that for $\Gamma = 0$ is 2.2 in the present configuration, but is 2.4 in the cylindrical configuration with a flat free surface. According to Ref. 16, the frequency decreases as the concavity of the free surface increases.

Based on the results of Figs. 3 and 4, if one has water in a 5-cm container, for example, the resonant frequencies are 0.67 and 1.47 Hz for $\Gamma = 0$ and 10,000, respectively. These values are the lowest resonant frequencies; in comparison, according to Ref. 15, the second resonant frequencies for the above water system are 3.45 and 4.40 Hz for $\Gamma = 0$ and 10,000, respectively. Those frequencies are all within a typical frequency range of g jitter aboard the Shuttle and Spacelab.[21]

Effects of g Jitter

In order to study the effect of g jitter, the fluid is subjected first to a simple harmonic g jitter in a direction parallel to the original flat free surface. The g jitter generates a time-dependent, nonuniform hydrostatic pressure field in the fluid, which must be balanced by the deformation of the free surface, resulting in a motion of the fluid. As at any given time the hydrostatic pressure distribution is linear in the g-jitter direction, it tends to generate a simple sloshing motion of the fluid from high- to low-pressure regions. Therefore, when the g-jitter frequency is approximately equal to the lowest resonant frequency previously discussed, the free-surface disturbance becomes large because the resonant motion is also a sloshing motion. On the other hand, when the g-jitter frequency is close to the second resonant frequency, it excites the second mode, but since the second mode is not simple sloshing motion,[15] an interaction between the second mode and the g-jitter-induced motion results in a complex motion but with a much smaller free-surface deformation than in the first case. For that reason we analyze mainly the first case in this work. The magnitude of harmonic g jitter aboard a spacecraft can be as large as $10^{-4}g_0$–$10^{-3}g_0$. If one considers a container dimension of 10 cm or smaller, the order of magnitude of Bo is unity or smaller for most common liquids and is in the range studied herein.

A simple velocity-vector plot is shown in Fig. 5 for $Bo = 0.25$, $Oh = 0.01$, $\Gamma = 1{,}000$, $\omega = 1.92$ (resonant frequency), and time = 5.76 (the fluid flow has been excited to the periodic steady state by this time). At that moment the body force acts from right to left (Fig. 5) and the fluid motion is strong enough to cause a visible free-surface deformation. Since the fluid motion is induced by the change in the free-surface shape, it occurs mainly near the surface. As shown in Fig. 5, most of the fluid motion occurs in the top half of the container, and the fluid in the bottom half is virtually unaffected by the g jitter. Since the contact lines are anchored in this case, not much fluid motion occurs near the contact lines. At $x = \frac{1}{4}$, the time history of the free-surface deformation in response to the above g jitter is shown in Fig. 6. In the case of inviscid flow, if the system is excited at the resonant frequency, the surface deformation will increase without bound, but in the present problem the excitation energy is eventually balanced by the viscous dissipation in the fluid, resulting in a finite deformation as seen in Fig. 6. It takes about 10 cycles to get to the periodic steady state at that Ohnesorge number ($Oh = 0.01$) but the number of cycles becomes smaller with increasing Oh. The largest positive deformation and negative deformation are not exactly equal, because of a small nonlinear effect. It can be shown that the ratio of nonlinear inertia terms to unsteady terms in Eqs. (2) and (3) is represented by the dimensionless free-surface deformation. As the deformation becomes large, the nonlinear effect becomes important. In the parametric ranges of the present analysis, the nonlinearity is relatively small, and its main effect is a slight difference in the peak and valley positions of the free surface, as seen in Fig. 6, which is found to occur when the dimensionless deformation becomes larger than about 1%.

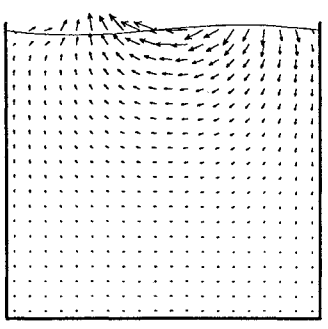

Fig. 5 Velocity vectors during g jitter. $Bo = 0.25$, $Oh = 0.01$, $\Gamma = 1000$, $\omega = 1.92$, t = 5.76 ($V_{max} = 0.071$)

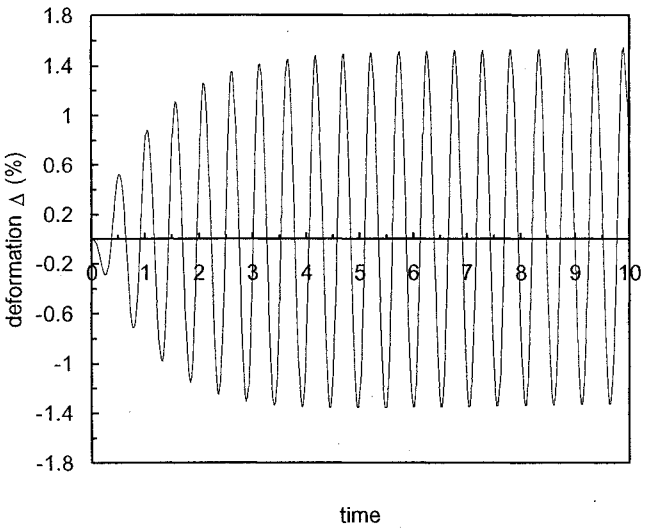

Fig. 6 Variation of free-surface deformation with time at resonant frequency with fixed contact line. $Bo = 0.25$, $Oh = 0.01$, and $\Gamma = 1000$.

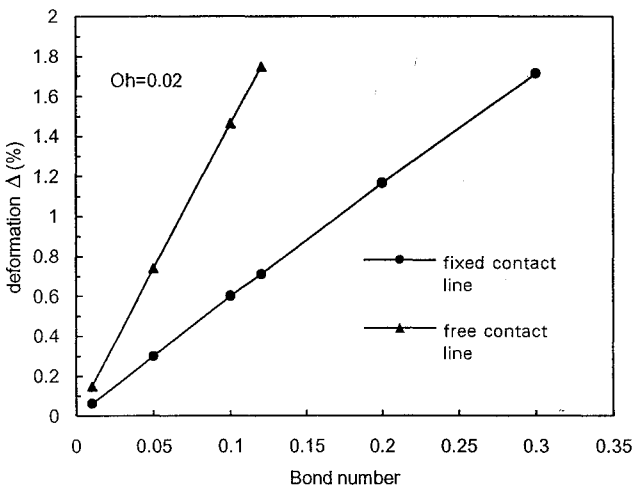

Fig. 7 Effect of Bond number on free-surface deformation.

In the subsequent discussion the amount of free-surface deformation is represented by the maximum value Δ in the periodic steady state. For large Γ the maximum free-surface deformation occurs near $x = \frac{1}{4}$ (Fig. 5), and for small Γ it occurs at the wall ($x = 0$). In Fig. 7, the Bond-number effect on the free-surface deformation is shown for two different-contact-line conditions with the excitation imposed at the corresponding resonant frequency. For a given Bo and Oh, the deformation increases with decreasing Γ as the increasingly free contact line makes it easier for the free surface to move. In the parametric ranges of the present investigation, the relation between the deformation and Oh is found to be linear, independent of the contact-line conditions. However, the present linear results are true only for relatively small deformation as in the present analysis. Much larger deformation results in nonlinear capillary waves. Consider, for example, 10-cS silicone oil in a 5-cm container. The resonant frequency is 0.83 Hz for the fixed-contact-line-condition and $Oh = 0.01$. If one wants to have the free-surface deformation be within ±2% of the container size, Bo should be less than 0.1 according to Fig. 7, or the g-jitter level should be less than about $10^{-4}g_0$. That level of g jitter is obtainable,[21] but it should be noted that the above estimation is

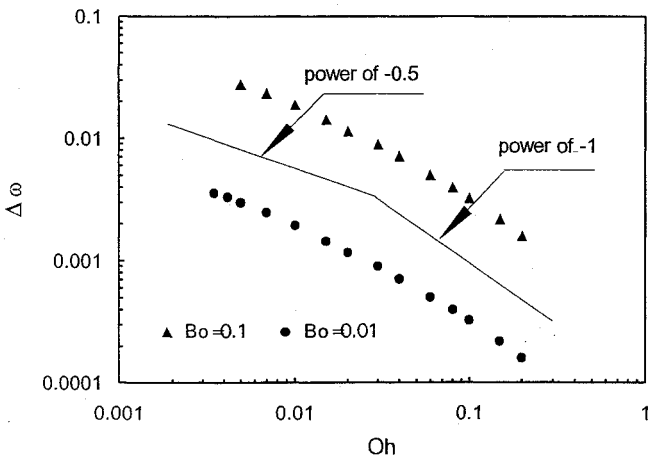

Fig. 8 Effect of Ohnesorge number on free-surface deformation for fixed contact line.

rather restrictive. It assumes that the sinusoidal g jitter at a particular frequency (0.83 Hz) lasts at that level for several cycles (at least 5 s), which may not be very realistic, depending on the particular spacecraft environment. For a small-viscocity, large-surface-tension fluid, such as water and liquid metals, Oh becomes very small, on the order of 10^{-4}. Although such small Oh is beyond the range of the present calculation because it results in a very thin boundary layer, it is clear that it will make the free surface much more sensitive to g jitter. Therefore, one needs to be very careful when designing a fluid system involving a free surface of such a fluid.

Figure 8 shows the effect of Ohnesorge number on free-surface deformation for two different Bond numbers and for $\Gamma = 1000$ at the resonant frequency (note that the ordinate is a logarithmic scale). In order to interpret the results in Fig. 8, the free-surface deformation is estimated by a scaling analysis as follows.

As was shown by Kamotani and Ostrach,[14] when the system is excited at the resonant frequency, the amount of deformation can be estimated by balancing the viscous stress ($\mu\, \partial v^*/\partial x^*$) at the wall and the hydrostatic pressure ($\rho A w^2 L$). The balance gives, after nondimensionlization, $v/\ell \sim Bo/Oh$, where ℓ is the length scale (relative to L) to estimate the viscous stress. Since the velocity v scales with $\Delta \cdot \omega$ during periodic oscillations, the above relation can be written as $\Delta \cdot \omega/\ell \sim Bo/Oh$. In the viscous-dominant case [$(Oh/\omega)^{\frac{1}{2}} \gg 1$], ℓ scales with the container size, namely $\ell \sim 1$, so the free-surface deformation during excitation at the resonant frequency is given by

$$\Delta \cdot \omega_n \sim \frac{Bo}{Oh} \tag{10}$$

In the boundary-layer flow case [$(Oh/\omega)^{\frac{1}{2}} \ll 1$], ℓ scales with the boundary-layer thickness, namely $\ell \sim (Oh/\omega)^{\frac{1}{2}}$, so the deformation is estimated as

$$\Delta \cdot \omega_n \sim \frac{Bo}{(Oh\omega_n)^{\frac{1}{2}}} \tag{11}$$

In both cases, Δ is proportional to Bo, as seen in Fig. 7. Equation (11) was also derived by Kamotani and Ostrach[14] for a cylindrical container. In Fig. 8 the ordinate is $\Delta\omega_n$. For a given Bo, $\Delta\omega_n$ scales with Oh^{-1} in the viscous case [Eq. (10)] and with $Oh^{-\frac{1}{2}}$ in the boundary-layer case [Eq. (11)]. As can be seen in Fig. 8, the present results cover both regions. The viscous estimate is applicable below $Oh = 0.1$, but, since the resonant frequency does not exist beyond $Oh = 0.3$ (Fig. 3), the viscous region is relatively small. Figure 8 indicates that the boundary-layer estimate can be used when Oh is below 5×10^{-3} or when $(Oh/\omega)^{\frac{1}{2}}$ is below about 0.05. The constant of proportionality for Eq. (11) is determined to be 0.03 from Fig. 8. In the drop-tower tests by Kamotani and Ostrach[14] with cylindrical containers, the proportionality constant was found to be 0.01. There are two reasons why the experimental value was

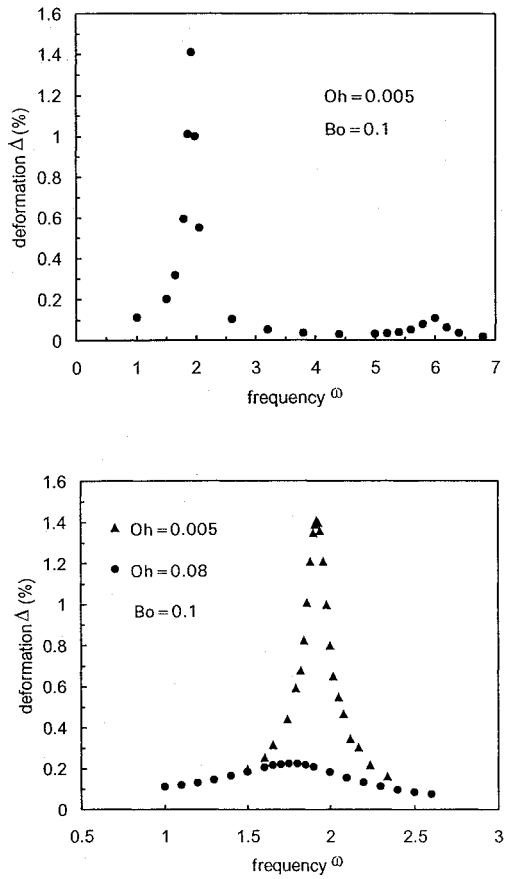

Fig. 9 Free-surface deformation as a function of g-jitter frequency for fixed contact line.

smaller. First, less than 2 s was available for microgravity in the tests, and the imposed frequencies were around 2 Hz, so that only four cycles were imposed, not enough to obtain the steady state, as Fig. 6 shows. Secondly, the configuration in the tests was cylindrical, which made the free surface more stable than in the two-dimensional configuration studied herein.

The g-jitter frequency versus the steady-state free-surface deformation for the fixed contact-line condition ($\Gamma = 1000$) is shown in Fig. 9a. If the system is disturbed at or near the resonant frequency, the free-surface deformation is very large. In that case the free-surface deformation increases with time until the steady state is reached (see Fig. 6), and the system can be said to be excited. The free-surface deformation near the resonant frequency is shown in Fig. 9b. The frequency range where the excitation occurs is narrow when Oh is small, but it broadens and the maximum deformation value decreases as the flow becomes more viscous (larger Oh). A second peak corresponding to the second wave mode can be identified in Fig. 9a at about $\omega = 5.9$, but with a much smaller magnitude than the first peak. On the other hand, if the system is disturbed at a frequency away from the resonant frequency, the deformation will be much smaller, and different characteristics of the free-surface response will be present. For example, in Fig. 10 the transient and steady responses of the free surface are shown when the system is forced at two non resonant frequencies [one above (Fig. 10a) and one below (Fig. 10b) the resonant frequency]. In both cases the resonant frequency is excited initially in addition to the g-jitter frequency. However, the transient response is quickly damped, and eventually the free surface oscillates with the frequency of the g jitter. Unlike Fig. 6 for the resonant case, the amplitude of surface deformation is now larger in the transient period. Since waves generated by higher-frequency g jitter experience larger viscous dissipation, the steady deformation in Fig. 10a is smaller than that in Fig. 10b, and the steady deformation in Fig. 10b is nearly equal to the transient deformation.

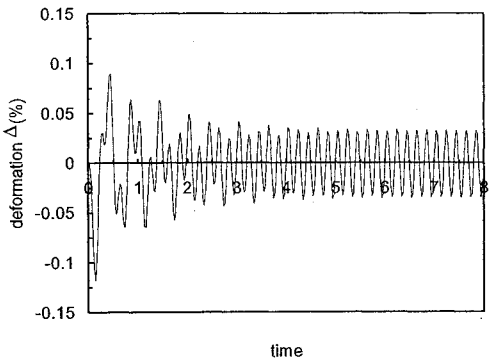

a) $\omega = 5.0$

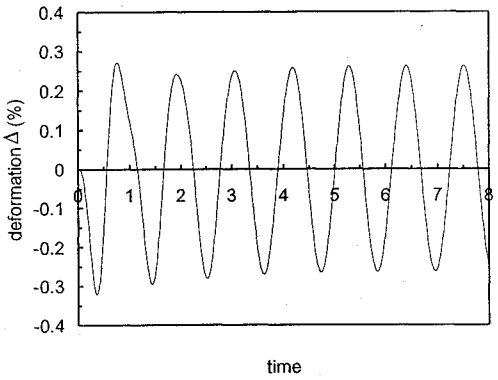

b) $\omega = 0.9$

Fig. 10 Variation of free-surface deformation with time at nonresonant frequencies for $Bo = 0.25$, $Oh = 0.02$, and $\Gamma = 1000$.

So far periodic g jitter has been discussed. The actual g jitter aboard a spacecraft may contain more than one frequency or a spectrum of frequencies. Although this case is not studied herein (a general treatment of that type of g jitter is difficult), it is clear from the above discussion that if the g jitter contains a frequency component at or near the resonant frequency, the free surface responds predominantly to that component and the deformation is relatively large. In that situation the amount of deformation can be estimated from the present results if the g jitter level associated with the frequency range where the excitation occurs (Fig. 9b) is used.

Another important type of g jitter is the impulse type. This type is characterized by short impulsive disturbances and caused by thruster firings for spacecraft altitude control and impulsive crew activity. In the present work, such g jitter is simulated by a constant acceleration of the container for a short period of time. The Bond number is now based on that acceleration level g. As will be shown later, the resonant frequency is excited by this g-jitter, so the non-dimensionalization of various quantities is done in the same way as in the periodic case. The fluid is considered to be quiescent up to time 0, when a constant acceleration (a constant Bo) is applied. The constant acceleration lasts up to time t_0 (dimensionless).

A typical free-surface response is presented in Fig. 11. The g-jitter excites waves at the resonant frequency, but their amplitude decays with time because of the viscous dissipation in the fluid. The impulsive g jitter accelerates the fluid and deforms the free surface. Even after the g jitter is stopped at t_0, the fluid keeps moving by its own inertia until the inertia is balanced by the surface-tension force, as in capillary waves, and the subsequent free-surface motion is that of capillary waves with the resonant frequency of the system. In this problem it is interesting to compute the maximum free-surface deformation (Δ_0), which occurs in the first cycle.

If the flow is nearly inviscid (small Oh) and if t_0 is of order $1/\omega_n$ (in that case the g jitter duration is comparable with the period of capillary waves), then by the time the g jitter ends, the free surface has enough time to deform as in capillary waves. In

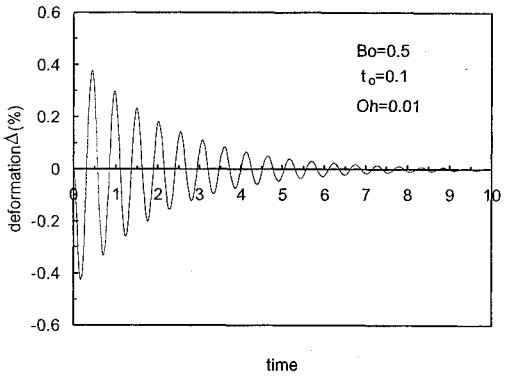

Fig. 11 Free-surface deformation for impulsive g jitter with fixed contact line.

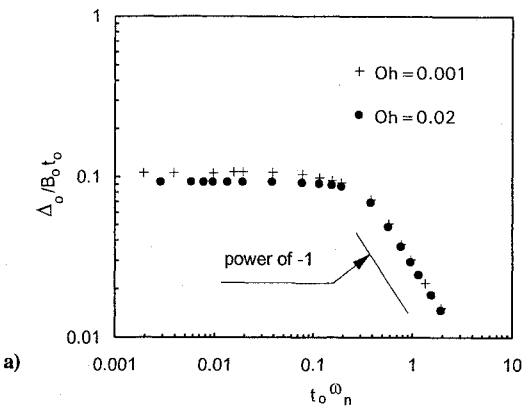

a)

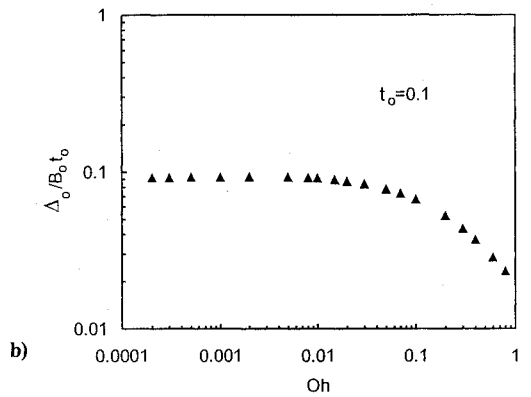

b)

Fig. 12 Correlation of maximum free-surface deformation for impulsive g jitter with fixed contact line.

that situation the surface shape is determined by a static balance between the hydrostatic pressure ($\rho g L$) and the capillary pressure ($\sigma \Delta_0^* L^2$), which gives a dimensionless relationship $\Delta \sim Bo$. If, on the other hand, t_0 is much smaller than $1/\omega_n$, the situation is now dynamic: the work done to the system by the g jitter is first converted to the kinetic energy of the fluid at time t_0, and the latter is eventually converted to the work done by the surface-tension force at the time the deformation becomes largest. Therefore, by balancing the input work $[(\rho L^2 g) \times (g \tau_0^2) = (\text{force}) \times (\text{distance})]$ and the work done during the free surface motion $[\sigma \Delta_0^{*2}/L]$, one obtains $\Delta_0 \sim Bo\, t_0$. If the flow is not inviscid, Δ_0 will also be a function of Oh.

In Fig. 12a, the computed $(\Delta_0/Bo\, t_0)$ is plotted against $t_0\omega_n$. As seen in the figure, when $t_0\omega_n$ is less than about 0.05, Δ_0 scales with $Bo\, t_0$, and when $t_0\omega_n$ is larger than about 0.5, Δ_0 scales with Bo. Figure 12b illustrates the influence of Oh on Δ_0 for a fixed t_0: the above inviscid estimate is valid up to about $Oh = 0.01$, but beyond

that, $\Delta_0/(Bot_0)$ decreases with increasing Oh, as a part of the input work is dissipated by viscosity.

The capillary waves thus generated decay with time (Fig. 11) as the total kinetic energy of the fluid decreases on account of viscous dissipation. By balancing the rate of change of the total kinetic energy of the fluid $[\rho L^2\, \partial u^{*2}/\partial t^*]$ and the total viscous dissipation in the fluid $[\mu(u^*/\ell)^2 L\ell]$, it can be shown that in the viscous case ($\ell \sim 1$) the free-surface deformation amplitude decreases as $\exp(-c\, Oh\, t)$, whereas in the boundary-layer case ($\ell^2 \sim Oh/\omega$) the amplitude decays as $\exp(-\bar{c}(Oh\,\omega)^{\frac{1}{2}} t)$. Based on the present computation, the value of c for viscous case is 23.0, and $\bar{c}$ for the boundary-layer case is 3.1.

Concluding Remarks

For a liquid placed in an open square container in microgravity, the free-surface deformation and the associated bulk fluid motion are computed numerically under various g-jitter and contact-line conditions. The results show that the free-surface deformation can be appreciable if the g jitter occurs near or at the resonant frequency for sloshing motion. Therefore, a liquid system with a free surface should be designed so that its resonant frequency does not coincide with the characteristic g jitter frequencies of the spacecraft, and if Oh of the system is larger than 0.001, one can use the present results to compute the amount of deformation in that situation. The g-jitter-induced flow occurs near the free surface. If the g-jitter is of the impulsive type, capillary waves with the resonant frequency are excited, but they decay with time. The present work predicts the maximum free-surface deformation for such g-jitter.

The motion and stability of a liquid free surface are an important problem in microgravity. In designing a fluid system with a free surface, the present result can be used to avoid unwanted disturbances due to g jitter aboard a spacecraft.

Acknowledgment

This work was funded by NASA through Grant NAG 3-886.

References

[1]Bauer, H. F., "Free Liquid Surface Response Induced by Fluctuations of Thermal Marangoni Convection," *AIAA Journal*, Vol. 22, No. 3, 1984, pp. 421–428.

[2]Ostrach, S., "Low Gravity Fluid Flows," *Annual Review of Fluid Mechanics*, Vol. 14, 1982, pp. 313–345.

[3]Abramson, H. M., 1963, "Dynamics Behavior of Liquid in Moving Container," *Applied Mechanics Review*, Vol. 16, No. 7, 1963, pp. 501–506.

[4]Lamb, H., *Hydrodynamics*, 6th ed., Dover, New York, 1945, pp. 363–475.

[5]Milne-Thomson, L. M., *Theoretical Hydrodynamics*, 5th ed., Macmillan, London, 1950, pp. 426–463.

[6]Penny, W. G., and Price, A. T., "Finite Periodic Stationary Gravity Waves in a perfect Liquid," *Philosophical Transactions of the Royal Society of London, Series A: Mathematical and Physical Sciences,* Vol. 244, 1952, pp. 254–284.

[7]Spradley, L. W., Bourgeois, S. W., and Lin, F. N., "Space Processing Convection Evaluation, g-Jitter Convection of Confined Fluids in Low Gravity," AIAA Paper 75-695, Jan. 1975.

[8]Kamotani, Y., Prasad, A., and Ostrach, S., "Thermal Convection in an Enclosure Due to Vibration aboard Spacecraft," *AIAA Journal*, Vol. 19, No. 4, 1981, pp. 511–516.

[9]Danabasoglu, G., and Biringen, S., "Computational of Convective Flow with g-Jitter in Rectangular Cavities," AIAA Paper 88-3727, June 1988.

[10]Curvelier, C., "A Capillary Free Boundary Problem Governed by the Navier-Stockes Equations," *Computer Methods in Applied Mechanics and Engineering*, Vol. 48, No. 2, 1985, pp. 45–80.

[11]Veldman, A. E. P., and Vogel, M. E. S., "Axisymmetrical Liquid Sloshing under Low-Gravity Conditions," *Acta Astronautica*, Vol. 11, No. 10/11, 1984, pp. 641–649.

[12]Ramachandran, N., "Effects of g-jitter and Marangoni Convection on Float Zones," *Journal of Spacecraft and Rockets*, Vol. 29, No. 4, 1992, pp. 514–522.

[13]Alexander, J. I. D., and Zhang, Y., "The Sensitivity of Non-isothermal Liquid Bridge to Residual Acceleration," *Microgravity Fluid Mechanics*, edited by H. J. Rath, Springer-Verlag, Berlin, 1992, pp. 167–174.

[14]Kamotani, Y., and Ostrach, S., "Design of a Thermocapillary Experiment in Reduced Gravity," *Journal of Thermophysics and Heat Transfer*, Vol. 1, No. 1, 1987, pp. 83–89.

[15]Chao, L., Ostrach, S., and Kamotani, Y., "Lateral g-Jitter Effects on Liquid Motion and Thermocapillary Convection in an Open Square Container under weightless condition," Case Western Reserve Univ., Rept. EMAE/TR 91-201, Cleveland, OH, Aug. 1991.

[16]Satterlee, H. M., and Reynolds, W. C., "The Dynamics of the Free Liquid Surface in Cylindrical Containers under Strong Capillary and Weak Gravity Conditions," Dept. of Mechanical Engineering, Stanford, Univ., Tech. Rept. LG-2, Stanford, CA, April 1964.

[17]Reynolds, W. C., and Satterlee, H. M., "Liquid Propellant Behavior at Low and Zero g," *The Dynamics Behavior of Liquids in a Moving Container*, NASA SP-106, 1966, Chap. 11, pp. 387–439.

[18]Hirt, C. W., and Nicholas, B. D., "SOLA—A Numerical Solution Algorithm for Transient Fluid Flow," Los Alamos Scientific Lab., Rept. LA 5852, Los Alamos, NM, 1975.

[19]Bulgarelli, U., Casulli, V., and Greenspan, D., *Pressure Methods for Numerical Solution of Free Surface Flows*, Pineridge Press, Swansea, Wales, UK, 1984, pp. 89–156.

[20]Schlichting, H., *Boundary Layer Theory*, 7th ed. McGraw-Hill, New York, 1979, pp. 93, 94.

[21]Baugher, C. R., Martin, G. L., and DeLombard, R., "Review of the Shuttle Vibration Environment," AIAA Paper 93-0832, Jan 1993.